

论文检索证明报告

论文作者：林哲、蔡恬、王燕锋

论文发表年限：2019

检索网站：SCI（科学引文索引, 2019）

检索方式：联机检索

检索结果：经检索，委托人于 2019 年发表的 1 篇文章被 SCI 收录。详见附件，特此证明。



厦门大学图书馆

2020 年 4 月 13 日

关闭

Web of Science
第 1 页 (记录 1 -- 1)

打印

◀[1]▶

第 1 条, 共 1 条

标题: Parallel reliability-guided algorithm for digital image correlation

作者: Lin, Z (Lin, Zhe); Cai, T (Cai, Tian); Wang, YF (Wang, Yanfeng)

来源出版物: INSIGHT 卷: 61 期: 12 页: 729-737 出版年: DEC 2019

Web of Science 核心合集中的 "被引频次": 0

被引频次合计: 0

使用次数 (最近 180 天): 1

使用次数 (2013 年至今): 1

引用的参考文献数: 28

摘要: Digital image correlation is a non-contact optical method for measuring the displacement and strain on the surface of a material. The existing reliability-guided digital image correlation (RG-DIC) method is stable and reliable for a single image but it still needs a large calculational resource for a sequence of images. Due to the decorrelation effect, the reference image must be replaced several times to correct the measurement results for an image sequence involving a large deformation or a discontinuous deformation. Since the process must be executed sequentially, image by image, the total time required is often unacceptably large when the image sequence is long. The challenge is to find a way of improving the speed while retaining calculational reliability and measurement accuracy, which are important for the practical application of DIC. To address this problem, an improved method is proposed in this paper. The parallel bottleneck caused by the decorrelation effect is solved through improving the parallelism to increase the processing speed. This approach can be used to calculate the strain field of the surface of the material in cases of discontinuous deformation, such as in the area near to a crack. Compared with existing methods, this method not only retains the calculational reliability but also greatly improves calculation speed, especially on current multi-core computing platforms.

入藏号: WOS:000503274000007

语言: English

文献类型: Article

KeyWords Plus: SYSTEMATIC-ERRORS; BEHAVIOR

地址: [Lin, Zhe] Shantou Polytech, Dept Comp, Shantou 515078, Peoples R China.

[Cai, Tian] Shantou Polytech, Network & Informat Ctr, Shantou 515078, Peoples R China.

[Wang, Yanfeng] Zhongyuan Univ Technol, Architectural Engn Inst, Zhengzhou 450007, Henan, Peoples R China.

通讯作者地址: Cai, T (通讯作者), Shantou Polytech, Network & Informat Ctr, Shantou 515078, Peoples R China.

电子邮件地址: tc45@126.com

出版商: BRITISH INST NON-DESTRUCTIVE TESTING

出版商地址: 1 SPENCER PARADE, NORTHAMPTON NN1 5AA, NORTHANTS, ENGLAND

Web of Science 类别: Instruments & Instrumentation; Materials Science, Characterization & Testing

研究方向: Instruments & Instrumentation; Materials Science

IDS 号: JW8CE

ISSN: 2156-485X

eISSN: 2156-4868

29 字符的来源出版物名称缩写: INSIGHT

ISO 来源出版物缩写: Insight

来源出版物页码计数: 9

基金资助致谢:

基金资助机构	授权号
Key Laboratory of Structure and Wind Tunnel of Guangdong Higher Education Institutes	201601 201803

The authors gratefully acknowledge the funding provided by the Key Laboratory of Structure and Wind Tunnel of Guangdong Higher Education Institutes (201601 and 201803).

输出日期: 2020-04-13

关闭

Web of Science
第 1 页 (记录 1 -- 1)

打印

◀[1]▶

Clarivate

Accelerating innovation

© 2020 Clarivate 版权通知 使用条款 隐私策略 Cookie 策略

登录以获取 Web of Science 时事新闻

关注我们



论文检索证明报告

论文作者：林哲、蔡恬、王燕锋

论文发表年限：2019

检索网站：EI（工程索引, 2019）

检索方式：联机检索

检索结果：经检索，委托人于 2019 年发表的 1 篇文章被 EI 收录。

详见附件，特此证明。



2020 年 4 月 13 日

1. Parallel reliability-guided algorithm for digital image correlation



Accession number: 20200107981854

Authors: Lin, Zhe (1); Cai, Tian (2); Wang, Yanfeng (3)

Author affiliation: (1) Department of Computer, Shantou Polytechnic, Shantou; 515078, China; (2) Network and Information Center, Shantou Polytechnic, Shantou; 515078, China; (3) Architectural Engineering Institute, Zhongyuan University of Technology, Zhengzhou; 450007, China

Corresponding author: Cai, Tian(tcai45@126.com)

Source title: Insight: Non-Destructive Testing and Condition Monitoring

Abbreviated source title: Insight Non Destr Test Cond Monit

Volume: 61

Issue: 12

Issue date: 2019

Publication year: 2019

Pages: 729-737

Language: English

ISSN: 13542575

E-ISSN: 17544904

CODEN: ITMOEN

Document type: Journal article (JA)

Publisher: British Institute of Non-Destructive Testing

Abstract: Digital image correlation is a non-contact optical method for measuring the displacement and strain on the surface of a material. The existing reliability-guided digital image correlation (RG-DIC) method is stable and reliable for a single image but it still needs a large calculational resource for a sequence of images. Due to the decorrelation effect, the reference image must be replaced several times to correct the measurement results for an image sequence involving a large deformation or a discontinuous deformation. Since the process must be executed sequentially, image by image, the total time required is often unacceptably large when the image sequence is long. The challenge is to find a way of improving the speed while retaining calculational reliability and measurement accuracy, which are important for the practical application of DIC. To address this problem, an improved method is proposed in this paper. The parallel bottleneck caused by the decorrelation effect is solved through improving the parallelism to increase the processing speed. This approach can be used to calculate the strain field of the surface of the material in cases of discontinuous deformation, such as in the area near to a crack. Compared with existing methods, this method not only retains the calculational reliability but also greatly improves calculation speed, especially on current multi-core computing platforms. © 2019 British Institute of Non-Destructive Testing. All rights reserved.

Number of references: 28

Main heading: Reliability

Controlled terms: Deformation - Image analysis - Optical correlation - Strain measurement

Uncontrolled terms: Calculation speed - Decorrelation effects - Digital image correlations - Discontinuous deformation - Measurement accuracy - Multi-core computing - Processing speed - Sequence of images

Classification code: 741.1 Light/Optics - 943.2 Mechanical Variables Measurements

DOI: 10.1784/insi.2019.61.12.729

Funding Details: Number: 201601, Acronym: -, Sponsor: Key Laboratory of Malignant Tumor Gene Regulation and Target Therapy of Guangdong Higher Education Institutes, Sun Yat-sen University;

Funding text: The authors gratefully acknowledge the funding provided by the Key Laboratory of Structure and Wind Tunnel of Guangdong Higher Education Institutes (201601 and 201803).

Compendex references: YES

Database: Compendex

Compilation and indexing terms: Copyright 2020 Elsevier Inc.

Data Provider: Engineering Village

Parallel reliability-guided algorithm for digital image correlation

Zhe Lin, Tian Cai and Yanfeng Wang

Digital image correlation is a non-contact optical method for measuring the displacement and strain on the surface of a material. The existing reliability-guided digital image correlation (RG-DIC) method is stable and reliable for a single image but it still needs a large calculational resource for a sequence of images. Due to the decorrelation effect, the reference image must be replaced several times to correct the measurement results for an image sequence involving a large deformation or a discontinuous deformation. Since the process must be executed sequentially, image by image, the total time required is often unacceptably large when the image sequence is long. The challenge is to find a way of improving the speed while retaining calculational reliability and measurement accuracy, which are important for the practical application of DIC. To address this problem, an improved method is proposed in this paper. The parallel bottleneck caused by the decorrelation effect is solved through improving the parallelism to increase the processing speed. This approach can be used to calculate the strain field of the surface of the material in cases of discontinuous deformation, such as in the area near to a crack. Compared with existing methods, this method not only retains the calculational reliability but also greatly improves calculation speed, especially on current multi-core computing platforms.

1. Introduction

Digital image correlation (DIC) has been widely used for measuring the displacement and strain on solid surfaces since 1980^[1]. It is an important experimental non-contact optical method used to monitor specimen deformation. In practice, DIC is used to measure the displacement and strain of the surface of a specimen during the loading process, in order to study the mechanical properties and failure law of the material. DIC has been applied to various materials, including heterogeneous materials^[2], biological materials^[3], wood^[4], shape memory alloys^[5], ceramics^[6], stone^[7], foam plastics^[8], etc.

In general, a fixed digital camera takes photographs of the same specimen surface twice at the moments just before and after specimen deformation. The two images are called the reference image and the deformed image, respectively. They are processed by a computer algorithm to determine the relative displacement at every point on the surface.

Over the past 30 years, a great effort has been made to improve the accuracy and efficiency of DIC. For example, Schreier *et al*^[9] achieved a measurement accuracy of 0.01 pixels by using higher-order spline interpolation functions. They also analysed the systematic errors that arise from the use of under-matched shape functions and investigated second-order shape functions in the matching process for non-uniform strain fields^[10]. Cheng *et al*^[11] presented an efficient, accurate and robust framework in which a uniform parametric B-spline surface function was used. By iterative optimisation, the unknown two-dimensional deformation field of the entire specimen surface area was obtained. Moreover, many studies on the search procedure^[12,13], the correlation approach^[14,15] and the registration method^[16-19] have been reported.

The existing reliability-guided digital image correlation (RG-DIC) method proposed by Pan^[20] is a stable and reliable method, but it still takes too much time when processing a sequence of images. In order to further improve the efficiency of the method, this paper proposes a parallel RG-DIC algorithm. Compared with the existing methods, it not only retains the calculational reliability,

but also greatly improves the calculation speed. It is also suitable for making full use of multi-core computing platforms to improve the processing efficiency of DIC.

2. Overview of digital image correlation

To obtain the full-field displacements, the first major task is to identify every point on the surface of the specimen. Usually, random speckle patterns are sprayed onto the surface of the specimen to ensure that the regions surrounding each point different from each other. As the specimen deforms, every region deforms as well.

In order to calculate the relative displacement at each point on the surface of the specimen, for each point of the deformed image the unique corresponding point is searched for in the reference image. Local characteristics of the surface of the specimen are used to determine the corresponding relationship between a pair of points. A subset with enough grey variation is chosen for each point in the reference image. Then, according to the predefined correlation criteria, an optimisation algorithm is used to find the most relevant subset in the deformed image. If the two subsets match successfully, the relative displacements of their central points constitute the displacement vector. As illustrated in Figure 1, the subset is chosen for the point in the deformed image and the corresponding point is tracked in the reference image according to grey intensity information.

● Submitted 06.12.18 / Accepted 25.07.19

Zhe Lin is with the Department of Computer, Shantou Polytechnic, Shantou 515078, China.

Tian Cai* is with the Network and Information Center, Shantou Polytechnic, Shantou 515078, China.

Yanfeng Wang is with the Architectural Engineering Institute, Zhongyuan University of Technology, Zhengzhou 450007, China.

*Corresponding author. Email: tc45@126.com

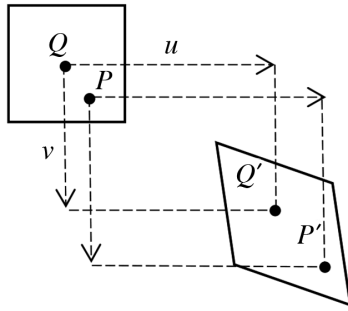


Figure 1. Subset deformation

In the subset, it is assumed that deformation is uniformly distributed, *ie* the displacement of points varies linearly in both horizontal and vertical directions, as mathematically described by the sharp function, as shown in Equation (1):

$$\begin{cases} u_p = u(x_{PQ}, y_{PQ}) \\ v_p = v(x_{PQ}, y_{PQ}) \end{cases} \dots (1)$$

where x_{PQ} and y_{PQ} are the distances from the point P to the subset centre Q in the horizontal and vertical directions, respectively. Using a first-order Taylor expansion, Equation (2) is obtained:

$$\begin{cases} \tilde{x}_{cur_p} = x_{ref_p} + u + \frac{\partial u}{\partial x}(x_{ref_p} - x_{ref_Q}) + \frac{\partial u}{\partial y}(y_{ref_p} - y_{ref_Q}) \\ \tilde{y}_{cur_p} = y_{ref_p} + v + \frac{\partial v}{\partial x}(x_{ref_p} - x_{ref_Q}) + \frac{\partial v}{\partial y}(y_{ref_p} - y_{ref_Q}) \end{cases} \dots (2)$$

where x_{ref_Q} and y_{ref_Q} represent the coordinates of Q in the reference image, x_{ref_P} and y_{ref_P} represent the coordinates of P in the reference image, x_{cur_p} and y_{cur_p} represent the coordinates of P in the deformed image and u and v are the displacements of Q in the x -direction and y -direction, respectively. Their partial derivatives are denoted by $\frac{\partial u}{\partial x}$, $\frac{\partial u}{\partial y}$, $\frac{\partial v}{\partial x}$ and $\frac{\partial v}{\partial y}$. The aim of DIC analysis is to find the optimal value of \vec{p} :

$$\vec{p} = \left\{ u, v, \frac{\partial u}{\partial x}, \frac{\partial u}{\partial y}, \frac{\partial v}{\partial x}, \frac{\partial v}{\partial y} \right\}^T \dots (3)$$

To evaluate the correlation between a $(2M+1) \times (2M+1)$ subset in the deformed image $g(x', y')$ and another one in the reference image $f(x, y)$, a correlation criterion is needed.

Many different correlation criteria have been reported in the literature, such as zero-mean cross-correlation (ZNCC)^[20,21]:

$$C_{ZNCC} = \sum_{i=-M}^M \sum_{j=-M}^M \left[\frac{\{f(x_i, y_j) - f_m\} \{g(x'_i, y'_j) - g_m\}}{\Delta f \Delta g} \right] \dots (4)$$

and least squares (LS)^[22,23]:

$$C_{LS} = \sum_{i=-M}^M \sum_{j=-M}^M \left[\frac{f(x_i, y_j) - f_m}{\Delta f} - \frac{g(x'_i, y'_j) - g_m}{\Delta g} \right]^2 \dots (5)$$

where:

$$f_m = \frac{1}{(2M+1)^2} \sum_{i=-M}^M \sum_{j=-M}^M f(x_i, y_j), \quad g_m = \frac{1}{(2M+1)^2} \sum_{i=-M}^M \sum_{j=-M}^M g(x'_i, y'_j) \dots (6)$$

$$\Delta f = \sqrt{\sum_{i=-M}^M \sum_{j=-M}^M [f(x_i, y_j) - f_m]^2}, \quad \Delta g = \sqrt{\sum_{i=-M}^M \sum_{j=-M}^M [g(x'_i, y'_j) - g_m]^2}$$

Based on Equations (2), (3) and (4), for every point an iterative optimisation algorithm, for example forward-additive Newton-Raphson (FA-NR)^[24,25] or inverse compositional Gauss-Newton

(IC-NG)^[26,27], is employed to find the optimal value of \vec{p} to maximise C_{ZNCC} or minimise C_{LS} .

3. Parallel reliability-guided algorithm

3.1 Reliability-guided algorithm

The pointwise scanning strategy, which is used by traditional DIC algorithms based on subsets, is difficult to use for specimens with geometric discontinuities or discontinuous deformation on the surface. In addition, it cannot accurately calculate boundary points since the subset around each boundary point contains unnecessary pixels, for example background pixels. To address the problem, Pan^[20] proposed RG-DIC, which has two main features.

The RG-DIC algorithm is different from traditional algorithms, which calculate points in line-by-line or column-by-column scanning. It uses an adaptive scanning path and computes points along the path with high correlation, instead of directly computing discontinuous points and boundary points. On the other hand, zero-mean normalised sum of squared difference (ZNSSD) criteria are revised when computing points on the boundary of the region of interest (ROI).

The flowchart of the RG-DIC algorithm is as follows. At the beginning, a queue Q is created and initialised to be empty. $W \times H$ binary matrices M_v and M_c are created, where W and H are the width and height of the reference image, respectively. The elements of M_v or M_c correspond to the points of the reference image. Every element of M_c is initialised to 0 and marked by 1 if the corresponding point has been computed.

- Step 1: Select a seed point (i, j) in the reference image as the starting point of the calculation, for which it is easy to find the corresponding point in the deformed image accurately and reliably. Next, the Newton-Raphson (NR) algorithm is used to calculate the correlation coefficient of the seed point, which is then inserted into queue Q . Finally, let $M_c(i, j) = 1$.
- Step 2: Pop the first point (represented as x_{ij}) of the queue Q , which is the point with the current highest correlation coefficient. If the adjacent point (represented as x_{ab}) of x_{ij} in the reference image satisfies:

$$\begin{cases} i-1 \leq a \leq i+1 \\ j-1 \leq b \leq j+1 \\ (i \neq a) \vee (j \neq b) \\ M_v(a, b) = 1 \\ M_c(a, b) = 0 \end{cases} \dots (7)$$

then the NR algorithm is used to calculate x_{ab} for the deformation parameters and correlation coefficient based on the calculation result of x_{ij} . After the calculation, x_{ab} is inserted into the queue Q corresponding to its correlation coefficient. $M_c(a, b) = 1$ is then set, since x_{ab} has been calculated.

- Step 3: Repeat the above steps until the queue Q is empty.

The RG-DIC algorithm calculates points according to correlation coefficient values. If a point has a low correlation coefficient value, its adjacent points are inserted into the end of queue Q for later calculation.

The RG-DIC method is robust and suitable for shadowed or discontinuous specimen surfaces; however, it still does not perform very well for large deformations. When the specimen undergoes large deformations, the shapes and positions of the subsets change

dramatically so that the patterns of speckle and texture become significantly different. As a result, the level of correlation between the corresponding subsets in the reference image and the deformed image decreases greatly; this is called the 'decorrelation effect'^[21].

3.2 The proposed parallel algorithm

Full-field strain measurement requires many calculations since it searches for the corresponding point after deformation for every point of the specimen surface. It is always difficult to find the best compromise between computational efficiency and measurement accuracy. Blaber *et al*^[22] used multi-threading to improve the RG-DIC algorithm and set multiple seed points. Each thread was responsible for a calculation path from a seed point.

As a local iterative optimisation algorithm, the IC-GN algorithm needs to select an initial estimated value close enough to the true value of the deformation at the beginning of the iteration. Therefore, the reliability-guided displacement tracking (RGDT) strategy in^[20] is guided by the ZNCC coefficients of the calculated points. However, the strategy is path dependent and is implemented in a serial manner point by point, which is wasteful and inefficient in modern multi-core computers. Therefore, an improved RGDT strategy is proposed in^[28], which uses a multi-threaded parallel computing method to process multiple pixels in parallel and greatly improve the calculation efficiency.

Although the method proposed in^[21] reduces the calculational error caused by the decorrelation effect, it is implemented to process the image sequence serially. When the correlation coefficient at the seed point is below the threshold, the reference image must be updated.

If the reference image is unchanged, the images in the deformed image sequence can be calculated respectively and in parallel. However, due to the decorrelation effect, the reference image may sometimes be replaced. Therefore, in order to obtain further parallelisation, the deformed image sequence is divided into several subsequences without the decorrelation effect.

The proposed algorithm preprocesses the image sequence quickly to predict the images that cause the decorrelation effect, rather than updating the reference images in the calculation process. The same correlation criterion C_{LS} as that used in^[22] is used for comparison. The reference image of every deformed image is determined in advance and the original image sequence is divided into several subsequences, each of which has its own reference image, so that all subsequences can be processed in parallel. The detailed process of the algorithm is described as follows:

- Step 1: Divide the sequence of images.

Firstly, the last image of the sequence is calculated.

Then, if the correlation coefficient at the seed point is smaller than a threshold value (0.8 in this case), which implies no decorrelation effect in the sequence of images, all of the deformed images can be processed in parallel, as in Step 3.

Otherwise, if the correlation coefficient at the seed point is equal to or larger than the threshold value, a binary search algorithm is employed to divide the sequence of images into two subsequences of equal length.

The binary division process is described as follows:

Define $T = \{I_{n=1, 2, \dots, N}\}$, which denotes the image sequence with length N .

Define the function:

$$F(T) = \mathbb{C}(I_N, I_1, s_x, s_y) \dots \dots \dots (8)$$

where $\mathbb{C}(I_p, I_r, s_x, s_y)$ represents the correlation coefficient at the point (s_x, s_y) , referring to the deformed image I_i and the reference image I_r .

Specifically, if $I_r = I_i$ then:

$$\mathbb{C}(I_r, I_r, s_x, s_y) = 0 \dots \dots \dots (9)$$

Since the correlation coefficient increases gradually, $\forall i, j \in (1, N)$:

$$i \geq j \Rightarrow \mathbb{C}(I_i, I_1, s_x, s_y) \geq \mathbb{C}(I_j, I_1, s_x, s_y) \dots \dots \dots (10)$$

and:

$$i \geq j \Rightarrow \mathbb{C}(I_N, I_j, s_x, s_y) \geq \mathbb{C}(I_N, I_i, s_x, s_y) \dots \dots \dots (11)$$

Assuming that $F(T) > \theta$, the sequence of images T is divided into two subsequences of equal length:

$$\Psi(T) \begin{cases} \{T_1, T_2\} & \text{if } F(T) > \theta \\ T & \text{else} \end{cases} \dots \dots \dots (12)$$

where T_1 and T_2 are the subsequences of T :

$$T_1 = \left\{ I_{n=1, 2, \dots, \lfloor \frac{N}{2} \rfloor} \right\} \dots \dots \dots (13)$$

$$T_2 = \left\{ I_{n=\lfloor \frac{N}{2} \rfloor + 1, \lfloor \frac{N}{2} \rfloor + 2, \dots, N} \right\} \dots \dots \dots (14)$$

If the binary division process is repeated p times, it can be described as:

$$\Psi^p(T) = \Psi(\Psi^{p-1}(T)) = \Psi(\{T_1, T_2, \dots, T_k\}) = \Psi(T_1) \cup \Psi(T_2) \cup \dots \cup \Psi(T_k) \dots (15)$$

where $p \in \mathbb{Z}^+$.

If p_0 is the minimum p that satisfies:

$$\Psi^{p+1}(T) = \Psi^p(T) \dots \dots \dots (16)$$

then the set of subsequences $\Psi^{p_0}(T)$ is the final result of the binary division.

A flowchart for solving $\Psi^{p_0}(T)$ is shown in Figure 2.

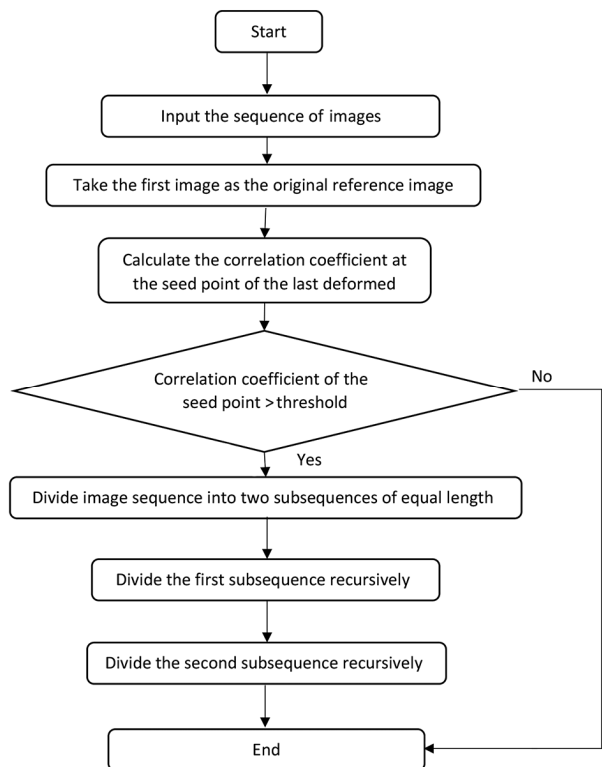


Figure 2. Recursive division of the sequence of images into subsequences

- Step 2: Take the last image of each subsequence as the reference image of the next subsequence. The displacement field of every reference image is calculated by the RG-DIC algorithm and then accumulated sequentially, as in Equation (17):

$$\vec{d}_j(x, y) = \vec{d}_{j, R(n)}(x, y) + \left[\sum_{m=2}^n \vec{d}_{R(m), R(m-1)}(x, y) \right] \dots (17)$$

where $\vec{d}_j(x, y)$ denotes the displacement vector of the j th image referring to the original reference image, $R(n)$ denotes the index of the reference image of the n th subsequence in the original image sequence and $\vec{d}_{ji}(x, y)$ denotes the displacement vector of the j th image referring to the i th image.

- Step 3: Calculate the displacement fields of all remaining deformed images in parallel. Every image is processed independently without communication with the others. In this way, the process can be implemented on a multi-core computing platform to make it run faster.

4. Results of trials

4.1 Trial using simulated results

The proposed method was evaluated on simulated speckle images, which were generated by a computer with a size of 512×512 pixels, as shown in Figure 3.

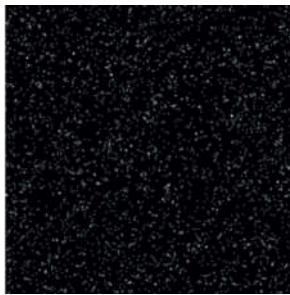


Figure 3. Simulated digital speckle image

Assuming the specimen was subjected to parallel pressure in the y -direction, axial compression occurred in the y -direction and axial stretching occurred in the x -direction, as shown in Figure 4. The grey box and the dotted frame represent the surface of the specimen before and after deformation, respectively. The Poisson ratio of the material was assumed to be 0.2. The displacement parameters of the specimen were assumed to be: $u_x = 0.02$, $v_y = -0.1$ and $u_y = v_x = 0$.

The change in the speckle image following deformation was simulated on the computer. In order to obtain images with large deformations, compression of the image was continued to generate a sequence of deformed images. The first one was compressed to 70% of the original image and the next deformed image was generated by further compression of 3%. Then, the same further compression

process was repeated until ten deformed images were obtained. The image before deformation was regarded as the original reference image (the 0th image). Figure 5 shows the reference (undeformed) image and the first deformed image.

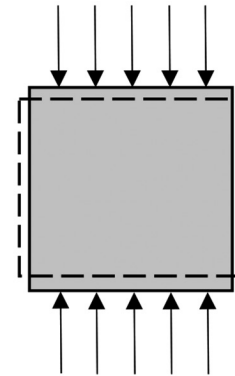


Figure 4. Deformation of the surface of the specimen

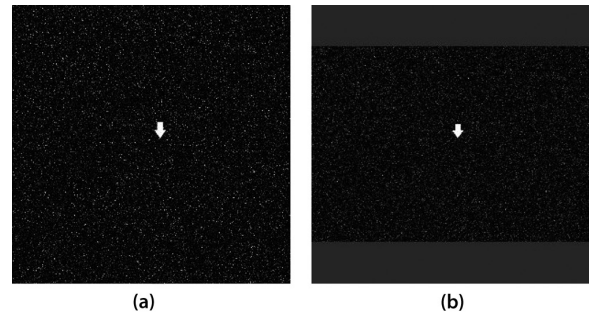


Figure 5. Large deformation of the simulated speckle image: (a) reference image; and (b) the first simulated image involving large deformation

The seed point was selected at (268, 248), which is indicated by the white arrows in Figure 5. The calculation process using the correlation criteria C_{LS} , which is defined by Equation (5), consisted of three iterations. The reference images and correlation coefficients are shown in Table 1.

As can be seen, in the first iteration, all the deformed images referred to the original reference image. It should be noted that the correlation coefficient increased significantly at the fifth deformed image, which indicates the decorrelation effect. As a result, in the second iteration, the original sequence was divided into two subsequences, where the 1st to 4th deformed images composed the first subsequence, which all referred to the original reference image and the correlation coefficients at the seed point remained unchanged; the 5th to 10th deformed images composed the second subsequence, which referred to the 4th deformed image and the

Table 1. Iterative processing of the sequence of images

Deformed image		1st	2nd	3rd	4th	5th	6th	7th	8th	9th	10th
Iteration 1	Reference image	0th	0th	0th	0th	0th	0th	0th	0th	0th	0th
	Correlation coefficient at the seed point	0.137	0.212	0.266	0.276	1.667	1.5	1.519	1.675	1.742	1.651
Iteration 2	Reference image	–	–	–	–	4th	4th	4th	4th	4th	4th
	Correlation coefficient at the seed point	–	–	–	–	0.11	0.131	0.155	0.156	0.175	1.498
Iteration 3	Reference image	–	–	–	–	–	–	–	–	–	9th
	Correlation coefficient at the seed point	–	–	–	–	–	–	–	–	–	0.13

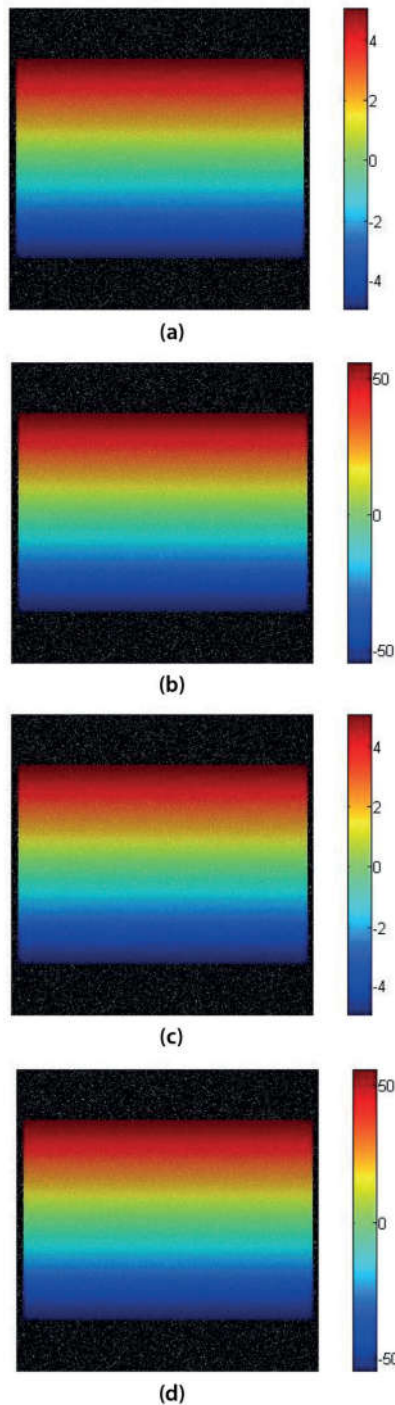


Figure 6. Displacement fields of the first and last deformed images: (a) displacement field of the first deformed image in the x-direction; (b) displacement field of the first deformed image in the y-direction; (c) displacement field of the last deformed image in the x-direction; and (d) displacement field of the last deformed image in the y-direction

recalculated correlation coefficients at the seed point were very small. The decorrelation effect can still be seen at the 10th image. For this reason, in the third iteration, the 10th deformed image referred to the 9th image and the correlation coefficient at the seed point was recalculated again. Finally, the displacement vector was obtained using Equation (18):

$$\vec{d}_j(x, y) = \begin{cases} \vec{d}_{j0}(x, y) & \text{if } 1 \leq j \leq 4 \\ \vec{d}_{j4}(x, y) + \vec{d}_{4,0}(x, y) & \text{if } 5 \leq j \leq 9 \\ \vec{d}_{j9}(x, y) + \vec{d}_{9,4}(x, y) + \vec{d}_{4,0}(x, y) & \text{if } j = 10 \end{cases} \quad \dots (18)$$

After calculation, the displacement fields of the first and last deformed images were obtained, as shown in Figure 6.

The calculation errors are shown in Table 2. The errors of the calculation results can be seen with respect to the expected values.

4.2 Plate hole 'DIC challenge'

A sequence of images, showing a plate hole sample from the Society for Experimental Mechanics (SEM)'s 'DIC challenge', which can be downloaded directly at <http://www.ncorr.com/download/sample12.zip>, are provided by ncorr.com to be used for testing and are taken from a real experiment in which a specimen with a hole in the middle is stretched in the y-direction, as shown in Figure 7. The image sequence contains one reference image and 11 deformed images. This sequence was used to evaluate the proposed method.

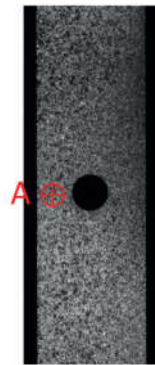


Figure 7. Reference image of the plate hole specimen

In order to analyse the calculation process in detail, Point A (90, 540) was taken, as shown in Figure 7. The final deformation vector $\vec{p} = (u, v, u_x, u_y, v_x, v_y)^T$ of the point was obtained after ten iterations.

Each iteration consisted of three key steps. Firstly, \vec{p} and $\Delta\vec{p}$ were used to calculate the corresponding relationship of pixels between the reference image and the deformed image. The grey values at subpixel positions (represented by $g(\vec{x} + W(\vec{\xi}; \vec{p}))$) of the deformed image were obtained by interpolation and then $\Delta\vec{p}$ was calculated by solving the equation $\nabla C = 0$ to minimise the correlation coefficient. Finally, \vec{p} was updated using $\Delta\vec{p}$. The process was repeated until the correlation coefficient converged to a

Table 2. Calculation errors of the trial using simulated results

	u	v	u_x	u_y	v_x	v_y
Expected result	0	0	0.02	0	0	-0.1
Calculation result	-0.03820592	-0.08769096	0.02049512	0.0191056	-0.00015962	-0.1036856
Absolute error	-0.03820592	-0.08769096	0.00049512	0.0191056	-0.00015962	-0.0036856
Relative error	-	-	2.5%	-	-	3.7%

global minimum. The details of $C(\Delta\bar{p})$, $\Delta\bar{p}$ and \bar{p} in the iterations are shown in Tables 3, 4 and 5, respectively.

Finally, the displacement fields in the x -direction and the y -direction of every point are shown in Figure 8.

To verify the reliability, the displacements at every point obtained by the proposed method and by the method in^[22] were compared. Table 6 shows the relative differences between the results of the two methods. It can be seen that the relative differences are all within 1%. The results of the two methods agree closely.

Table 3. Correlation coefficient $C(\Delta\bar{p})$ of Point A in the iterations of the plate hole 'DIC challenge'

Iteration	$C(\Delta\bar{p})$
1	0.07596317
2	0.00300894
3	0.00289571
4	0.00289574
5	0.00289573

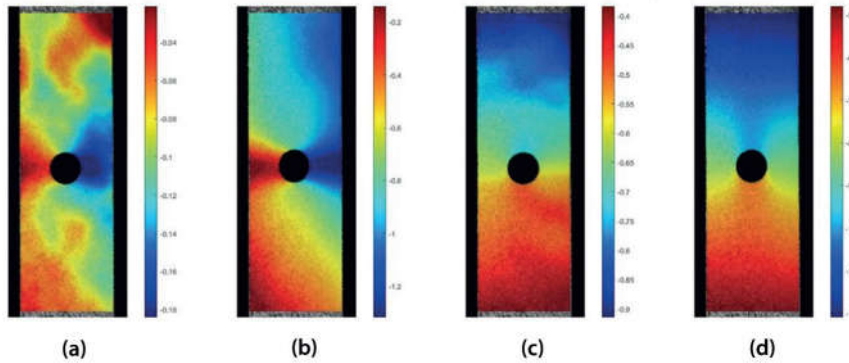


Figure 8. Displacement fields in the x -direction and in the y -direction of every point of the sample used in the plate hole 'DIC challenge': (a) displacement field in the x -direction of every point of the first deformed image; (b) displacement field in the x -direction of every point of the last deformed image; (c) displacement field in the y -direction of every point of the first deformed image; and (d) displacement field in the y -direction of every point of the last deformed image

Table 4. $\Delta\bar{p}$ of Point A in the iterations of the plate hole 'DIC challenge'

Iteration	$\Delta\bar{p}$					
1	0.03193411	-0.3742756	0.00014554	0.00031882	0.00000056	-0.00031427
2	0.00106199	-0.01501222	-0.00008576	0.00001449	0.0000034	0.00011715
3	0.00006395	0.00021812	-0.00000309	-0.00000376	0.00000399	-0.00000173
4	-0.00000048	-0.00000355	0.00000003	0.00000002	-0.00000011	0.00000004
5	0.00000001	0.00000006	0.00000000	0.00000000	0.00000000	0.00000000

Table 5. \bar{p} of Point A in the iterations of the plate hole 'DIC challenge'

Iteration	\bar{p}					
1	-0.03204881	-0.6256067	-0.00014552	-0.00031888	-0.00000056	0.00031437
2	-0.03311574	-0.6105915	-0.00005976	-0.00033333	-0.00000396	0.00019719
3	-0.03317961	-0.6108097	-0.00005667	-0.00032956	-0.00000795	0.00019893
4	-0.03317914	-0.6108061	-0.00005671	-0.00032959	-0.00000784	0.00019889
5	-0.03317915	-0.6108062	-0.00005671	-0.00032958	-0.00000784	0.00019889

Table 6. Relative differences between the results of two methods

Deformed image	Maximum difference (%)	Mean difference (%)	Minimum difference (%)
1	0.38	0.32	0.27
2	0.51	0.51	0.47
3	0.54	0.53	0.46
4	0.54	0.45	0.42
5	0.68	0.66	0.64
6	0.7	0.66	0.64
7	0.86	0.75	0.66
8	0.97	0.83	0.73
9	0.96	0.84	0.74
10	0.97	0.81	0.77

4.3 Three-point bending test

The proposed method was also evaluated on a sequence of images from a three-point bending test in the materials laboratory of Shantou University. The equipment is shown in Figure 9. The loading equipment is a SANS universal testing machine, as shown in Figures 9(a) and 9(b), which can apply a maximum test force of 100 kg. A Revealer 5F04 high-speed camera, produced by Hefei Fuhuang Junda High-Tech Information Technology Co Ltd, was used to photograph the specimen, as shown in Figure 9(c). Its frame rate reached 500 FPS at full resolution (2320×1720).

The experimental steps were as follows:

- Step 1: A concrete specimen with a flat surface was selected, the size of which was $20 \text{ cm} \times 5 \text{ cm}$. The surface was sprayed with white matte paint and then irregular black spots were applied. A 2 cm-long crack was fabricated in the y -direction and in the middle of the x -direction of the specimen, as shown in Figure 10.

- Step 2: The specimen was placed horizontally and symmetrically on the universal testing machine, the press ram was moved to the horizontal centre of the test block and the camera was adjusted to achieve a clear image.
- Step 3: An image was taken as the reference image before deformation, as shown in Figure 11. Then, the universal testing machine was controlled by a computer to slowly increase the load so that the prefabricated crack gradually expanded upward until the specimen was completely broken. Finally, 11 test images were extracted from the image sequence captured by the camera and sent for DIC calculation.

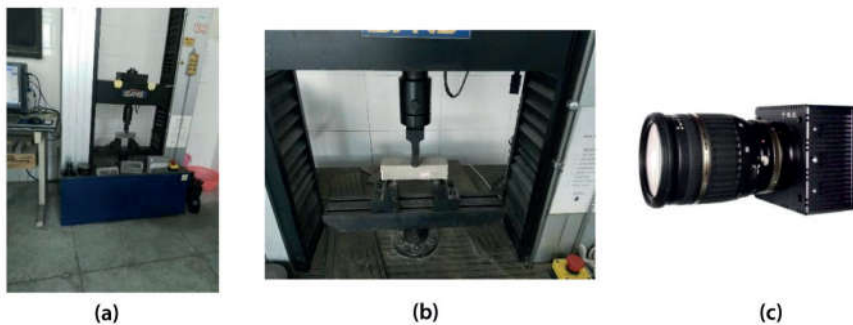


Figure 9. Experimental equipment for the three-point bending test: (a) and (b) SANS universal testing machine; and (c) high-speed camera 5F04

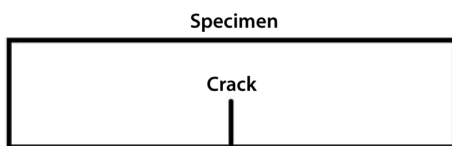


Figure 10. Specimen with a prefabricated crack



Figure 11. Reference image in the three-point bending test

Figure 12 shows the final calculational results for the points. In order to save space, only the first and the last deformed images are shown, as in Figures 12(a) and 12(b), respectively. Figures 12(c) and 12(d) are the corresponding displacement figures in the x -direction, where blue represents negative displacement (a move left) and red represents positive displacement (a move right). It can be seen that as the load increased and the crack grew, the left-hand and right-hand parts of the specimen moved towards the two sides. There is a clear separation line between the blue part and the red part, which is the opening crack. In addition, the deeper the colour is, the larger the displacement is. Comparing Figures 12(c) and 12(d), it is interesting to note that the crack tip has clearly moved upwards.

4.4 Acceleration effect

The computing run-times of the proposed method in these trials are shown in Table 7. It can be seen that the computing speed of the proposed method has increased by more than 50% compared with the method in^[22].

5. Conclusions

This paper has presented an improved reliability-guided digital image correlation method, in which correlation coefficients at seed points are used to determine the position of the decorrelation effect and recursively divide the sequence of images into several subsequences. Next, a multi-process parallel algorithm is used to process the subsequences simultaneously and the final calculation results are obtained by accumulation. Based on existing methods, this method not only uses multi-threading computation to improve the pixel-level parallelism when processing an image but it also uses multi-process computation to achieve image-level parallelism.

The main advantage of this method is that it rapidly eliminates the decorrelation effect inside the sequence of images by recursively dividing the image into subsequences. The method can calculate the displacement field of a material surface subjected to large deformation more quickly than other methods and is suitable for analysing the process of fracture.

Compared with existing methods, this method is not only reliable but also more efficient. It uses multi-core calculations to make full use of advanced computing resources to improve the processing efficiency of DIC. In addition, the method is compatible with the existing multi-thread acceleration method.

The following future work is needed to improve the proposed method. Firstly, the automatic selection of the best seed point is still a problem. The location of the seed point has a great influence on the recursive division of the image sequence. The selection of seed points is still performed manually and is the key to the proposed method. Automatic selection of the seed points is essential for automatic real-time application.

Secondly, the robustness of the proposed method in the outdoor environment needs to be improved. Since outdoor light is not stable, the images output by a camera will fluctuate significantly and the maintenance of the measuring accuracy and reliability of DIC will be of practical significance but present a challenge for further research.

Finally, the best method for determining the number of image subsequences for a specific computing platform needs to be found, which is another important factor in achieving optimal overall performance.

Acknowledgements

The authors gratefully acknowledge the funding provided by the Key Laboratory of Structure and Wind Tunnel of Guangdong Higher Education Institutes (201601 and 201803).

References

1. W H Peters and W F Ranson, 'Digital imaging techniques in experimental stress analysis', *Optical Engineering*, Vol 21, No 3, pp 427-431, 1982.
2. G Sierra, B Watrisse and C Bordreuil, 'Structural analysis of steel to aluminium welded overlap joint by digital image correlation', *Experimental Mechanics*, Vol 48, No 2, pp 213-223, 2008.
3. N Bahlouli, S M'Guil, S Ahzi and M Laberge, 'Stress-strain response of biomaterials by a digital image correlation method: application to Tecoflex', *Journal of Materials Science Technology*, Vol 20, pp 114-116, 2004.

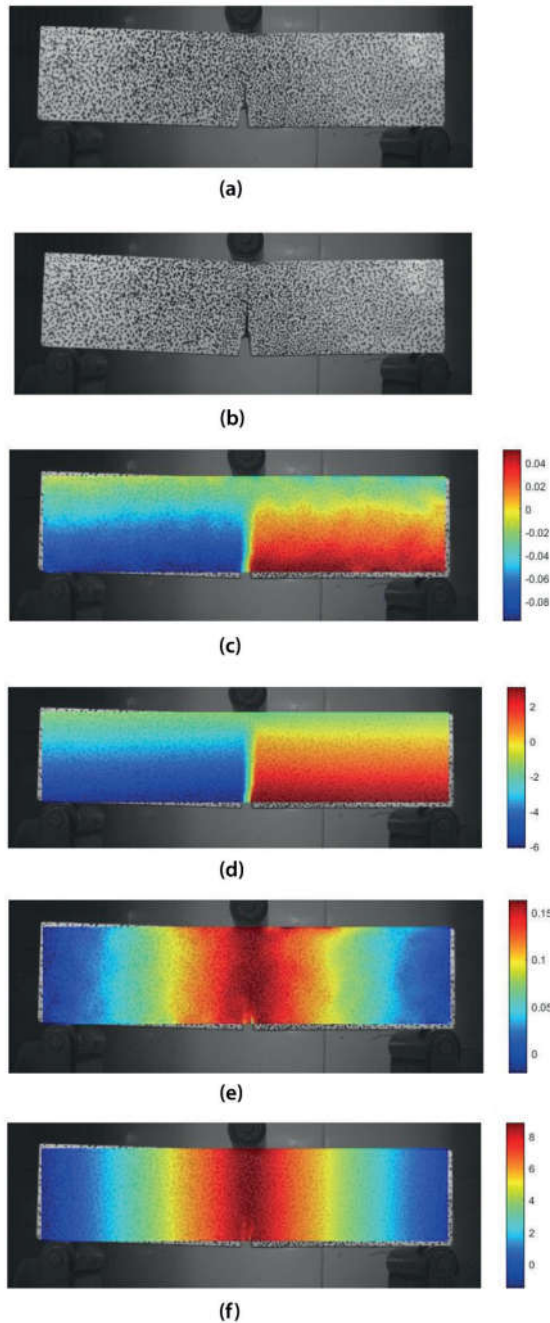


Figure 12. Displacement in the x -direction and in the y -direction of every point in the three-point bending test: (a) the first deformed image; (b) the last deformed image; (c) displacement field in the x -direction of every point of the first deformed image; (d) displacement field in the x -direction of every point of the last deformed image; (e) displacement field in the y -direction of every point of the first deformed image; and (f) displacement field in the y -direction of every point of the last deformed image

Table 7. Comparison of computing run-times

Experiment	Number of deformed images	Time consumed by the method in ^[22] (s)	Time consumed by the proposed method (s)	Speed-up (%)
Plate hole 'DIC challenge'	11	547	335	163
Three-point bending test	11	919	612	150

- S Ukyo and M Masuda, 'Investigation of the true stress-strain relation in shear using the digital image correlation method', *Journal of the Japan Wood Research Society*, Vol 50, No 3, pp 146-150, 2004.
- H A Bruck, C L Moore and T M Valentine, 'Bending actuation in polyurethanes with a symmetrically graded distribution of one-way shape memory alloy wires', *Experimental Mechanics*, Vol 44, No 1, pp 62-70, 2004.
- V Huon, B Wattrisse, M S E Youssoufi and A Chrysochoos, 'Elastic behaviour of anisotropic terracotta ceramics determined by kinematic full-field measurements', *Journal of the European Ceramic Society*, Vol 27, No 5, pp 2303-2310, 2007.
- A R Bhandari and J Inoue, 'Experimental study of strain rates effects on strain localisation characteristics of soft rocks', *Journal of the Japanese Geotechnical Society*, Vol 45, No 1, pp 125-140, 2005.
- H Jin, W Lu, S Scheffl, T D Hinnerichs and M K Neilsen, 'Full-field characterisation of mechanical behaviour of polyurethane foams', *International Journal of Solids and Structures*, Vol 44, No 21, pp 6930-6944, 2007.
- H W Schreier, J R Braasch and M A Sutton, 'Systematic errors in digital image correlation caused by intensity interpolation', *Optical Engineering*, Vol 39, No 11, pp 2915-2921, 2000.
- H W Schreier and M A Sutton, 'Systematic errors in digital image correlation due to undermatched subset shape functions', *Experimental Mechanics*, Vol 42, No 3, pp 303-310, 2002.
- P Cheng, M A Sutton, H W Schreier and S R McNeill, 'Full-field speckle pattern image correlation with B-spline deformation function', *Experimental Mechanics*, Vol 42, No 3, pp 344-352, 2002.
- R S He, C T Horn, H J Wang and S F Hwang, 'Deformation measurement by a digital image correlation method combined with a hybrid genetic algorithm', *Key Engineering Materials*, Vol 326-328, pp 139-142, 2006.
- Z Zhang, Y Kang, H Wang, Q Qin, Y Qiu and X Li, 'A novel coarse-fine search scheme for digital image correlation method', *Measurement*, Vol 39, No 8, pp 710-718, 2006.
- Z Hou and Y Qin, 'The study of fractal correlation method in the displacement measurement and its application', *Optics and Lasers in Engineering*, Vol 39, No 4, pp 465-472, 2003.
- H Jin and H A Bruck, 'Pointwise digital image correlation using genetic algorithms', *Experimental Techniques*, Vol 29, No 1, pp 36-39, 2010.
- C Tang, H Zuo, D Yun, C Xing and H Zhang, 'A new synthetical algorithm for digital image correlation method and its application in the fracture', *Optical Technique*, No 1, pp 69-72, 2003.
- Y Sun, J H L Pang and C K Wong, 'Finite element formulation for a digital image correlation method', *Applied Optics*, Vol 44, No 34, pp 7357-7363, 2005.
- B Pan and H M Xie, 'Digital image correlation method with differential evolution', *Journal of Optoelectronics · Laser*, Vol 18, No 1, pp 100-103, 2007.
- Y Sun and J H L Pang, 'Study of optimal subset size in digital image correlation of speckle pattern images', *Optics and Lasers in Engineering*, Vol 45, No 9, pp 967-974, 2007.
- B Pan, 'Reliability-guided digital image correlation for image deformation

- measurement', *Applied Optics*, Vol 48, No 8, pp 1535-1542, 2009.
21. B Pan, D Wu and Y Xia, 'Incremental calculation for large deformation measurement using reliability-guided digital image correlation', *Optics and Lasers in Engineering*, Vol 50, No 4, pp 586-592, 2012.
 22. J Blaber, B Adair and A Antoniou, 'Ncorr: open-source 2D digital image correlation MATLAB software', *Experimental Mechanics*, Vol 55, No 6, pp 1105-1122, 2015.
 23. P Bing, H Xie, Z Guo and H J O E Tao, 'Full-field strain measurement using a two-dimensional Savitzky-Golay digital differentiator in digital image correlation', *Optical Engineering*, Vol 46, No 3, 033601, 2007.
 24. H A Bruck, S R McNeill, M A Sutton and W H Peters III, 'Digital image correlation using Newton-Raphson method of partial differential correction', *Experimental Mechanics*, Vol 29, No 3, pp 261-267, 1989.
 25. B Pan, H-M Xie, B-Q Xu and F-L Dai, 'Performance of subpixel registration algorithms in digital image correlation', *Measurement Science and Technology*, Vol 17, No 6, p 1615, 2006.
 26. B Simon and M Iain, 'Equivalence and efficiency of image alignment algorithms', *Proceedings of the 2001 IEEE Conference on Computer Vision and Pattern Recognition (CVPR 2001)*, Kauai, Hawaii, 8-14 December 2001.
 27. T Li, 'Fast, robust and accurate digital image correlation calculation without redundant computations', *Experimental Mechanics*, Vol 53, No 7, pp 1277-1289, 2013.
 28. B Pan and L Tian, 'Superfast robust digital image correlation analysis with parallel computing', *Optical Engineering*, Vol 54, No 3, 034106, 2015.